Resonant control of stochastic spatiotemporal dynamics in a tunnel diode by multiple time-delayed feedback

Niels Majer and Eckehard Schöll*
Institut für Theoretische Physik, Technische Universität Berlin, D-10623 Berlin, Germany
(Received 30 August 2008; published 12 January 2009)

We study the control of noise-induced spatiotemporal current density patterns in a semiconductor nanostructure (double-barrier resonant tunneling diode) by multiple time-delayed feedback. We find much more pronounced resonant features of noise-induced oscillations compared to single time feedback, rendering the system more sensitive to variations in the delay time τ. The coherence of noise-induced oscillations measured by the correlation time exhibits sharp resonances as a function of τ, and can be strongly increased by optimal choices of τ. Similarly, the peaks in the power spectral density are sharpened. We provide analytical insight into the control mechanism by relating the correlation times and mean frequencies of noise-induced breathing oscillations to the stability properties of the deterministic stationary current density filaments under the influence of the control loop. Moreover, we demonstrate that the use of multiple time delays enlarges the regime in which the deterministic dynamical properties of the system are not changed by delay-induced bifurcations.

DOI: 10.1103/PhysRevE.79.011109 PACS number(s): 05.40.−a, 05.45.−a, 72.20.Ht, 72.70.+m

I. INTRODUCTION

It is well known that random fluctuations can seriously affect charge transport in semiconductors [1], which usually leads to deterioration of their performance. However, recently the constructive role of noise in semiconductor devices has been recognized. In particular, noise was shown to induce coherent radiation in semiconductor lasers [2–4] or to induce moving field domains in semiconductor superlattices [5] whose regularity becomes optimum at some nonzero value of the noise intensity. This phenomenon is known as *coherence resonance* [6,7]. In double-barrier resonant tunneling (DBRT) diodes noise can generate spatially inhomogeneous current density patterns in the form of breathing current filaments [8], however, their regularity decreases monotonically with increasing noise intensity, and thus shows no coherence resonance.

The control of the features of noise-induced dynamics is generally of great importance, and has recently attracted a lot of attention in the field of nonlinear dynamic systems [9]. In [10,11] a method for manipulation of essential features of noise-induced oscillations, such as coherence and time scales, was proposed using a delayed feedback scheme that was originally used to control chaos in purely deterministic systems [12]. This technique was demonstrated to be effective for control of noise-induced oscillations in either simple (generic) systems [13–18] or more complex, spatially extended systems [19–21]. For the DBRT nanostructure it was shown that time-delayed feedback can either increase or decrease the regularity of noise-induced breathing filaments and, moreover, can even lead to spatial homogenization of current density patterns [22]. For deterministic systems the original *single* time-delayed feedback was extended by using multiples of the delay time τ weighted with a memory parameter [23], which generally leads to larger control domains and more efficient control [24–27]. In a simple stochastic Van der Pol oscillator this has also been shown to yield drastically increased correlation times [28].

In the present work we study the effect of *multiple* time-delayed feedback on the stochastic spatiotemporal pattern formation in the DBRT model. Compared to the single time-delayed feedback in the same system [22], we find much sharper resonances of the spectral and correlation properties in dependence upon the delay time. For parameter values close to, but below a Hopf bifurcation we show that in these sharp, pronounced resonances the temporal regularity is significantly increased and the power spectral width becomes much narrower. Moreover, we demonstrate that the use of multiple time delays enlarges the control parameter regime in which the original deterministic dynamical properties of the system do not change, i.e., the delay-induced bifurcations occur only at larger feedback strength.

The paper is organized as follows. In Sec. II the DBRT model is described, and the dynamical properties of the system for our chosen parameters are discussed. Section III is devoted to the effects of the multiple time-delayed feedback upon noise-induced dynamics, and in Sec. IV we draw conclusions.

II. MODEL

In our study, we use a deterministic model for the DBRT suggested in [29] and add two sources of random fluctuations as proposed in [8]. Furthermore, we use the time-delayed feedback scheme, which was already applied to this system in [22], and extend it in order to take multiple time intervals into account in the feedback loop.

$$\frac{\partial a(x,t)}{\partial t} = f(a,u) + \frac{\partial}{\partial x}\left(D(a)\frac{\partial a}{\partial x}\right) + D_a\xi(x,t),$$

$$\frac{\partial u(t)}{\partial t} = \frac{1}{\varepsilon}(U_0 - u - rJ) + D_u\eta(t) + F(t), \qquad (1)$$

*schoell@physik.tu-berlin.de

where all quantities are dimensionless. The dynamical variable $a(x,t)$ describes the charge carrier density inside the quantum well, whereas $u(t)$ is the voltage drop across the device. The spatial coordinate x denotes the direction perpendicular to the current flow, and t is time. In terms of nonlinear dynamics, in the deterministic ($D_a=D_u=0$) and uncontrolled ($K=0$) case, this is a reaction-diffusion model of the activator-inhibitor type, where a is the activator, and u is the inhibitor [30].

The net tunneling rate of the electrons through the two energy barriers into and out of the quantum well is modeled by the nonlinear function [29]

$$f(a,u) = j_{in} - j_{out},$$

$$j_{in} = \left\{ \frac{1}{2} + \frac{1}{\pi} \arctan\left[\frac{2}{\gamma}\left(x_0 - \frac{u}{2} + \frac{d}{r_B} a \right) \right] \right\} \times \left\{ \ln\left[1 + \exp\left(\eta_e - x_0 + \frac{u}{2} - \frac{d}{r_B} a \right) \right] - a \right\},$$

$$j_{out} = a, \tag{2}$$

where d is the effective thickness of the double-barrier structure, $r_B=(4\pi\epsilon\epsilon_0\hbar^2)/(e^2m)$ is the effective Bohr radius in the semiconductor material, ϵ and ϵ_0 are the relative and absolute permittivity of the material, and x_0 and γ describe the energy level and the broadening of the electron states in the quantum well and η_e is the dimensionless Fermi level in the emitter, all in units of k_BT. Throughout the paper we use values of $\gamma=6$, $d/r_B=2$, $\eta_e=28$, and $x_0=114$, corresponding to typical device parameters at 4 K [29].

The effective diffusion coefficient $D(a)$ resulting from the inhomogeneous lateral redistribution of carriers and from the change in the local potential due to the charge accumulated in the quantum well by Poisson's equation is given by [31]

$$D(a) = a\left(\frac{d}{r_B} + \frac{1}{1-\exp(-a)} \right). \tag{3}$$

It describes the diffusion of the electrons within the quantum well perpendicular to the current flow. $J=\frac{1}{L}\int_0^L j dx$ gives the total current through the device, where $j(a,u)=\frac{1}{2}(j_{in}+j_{out})=\frac{1}{2}[f(a,u)+2a]$ is the local current density within the well. The system's width is fixed at a value of $L=30$ and homogeneous Neumann boundary conditions are used.

In Eq. (1) we use uncorrelated Gaussian white noise sources $\xi(x,t)$ and $\eta(t)$ with noise intensities D_a and D_u

$$\langle \xi(x,t) \rangle = \langle \eta(t) \rangle = 0 \quad (x \in [0,L]),$$

$$\langle \xi(x,t)\xi(x',t') \rangle = \delta(x-x')\delta(t-t'),$$

$$\langle \eta(t)\eta(t') \rangle = \delta(t-t'). \tag{4}$$

Physically, D_u can be realized by an external tunable noise voltage source in parallel with the supply bias. D_a describes internal fluctuations of the local current density, which could be caused, e.g., by shot noise [1].

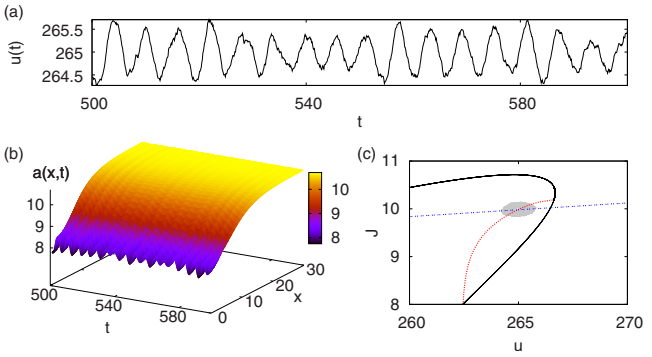

FIG. 1. (Color online) Stochastic spatiotemporal dynamics under multiple time-delayed feedback control. (a) Voltage time series $u(t)$ (in units of 0.35 mV), (b) charge carrier density $a(x,t)$ (in units of $10^{10}/\mathrm{cm}^2$), (c) phase portrait of current J (in units of 500 A/cm^2) vs voltage u. Space x and time t are scaled in units of 100 nm and 3.3 ps, respectively, corresponding to typical device parameters at 4 K [29]. Parameters are $U_0=-84.2895$, $r=-35$, $\varepsilon=6.2$, $D_u=0.1$, $D_a=10^{-4}$, $K=0.1$, $\tau=6.3$, $R=0.5$.

The control force $F(t)$ represents a control voltage, which is constructed recursively from a time-delayed feedback loop with delay time τ, feedback strength $K \geqslant 0$, and memory parameter R, and can be written as

$$F(t) = K[u(t-\tau) - u(t)] + RF(t-\tau) \tag{5}$$

$$= K\sum_{n=0}^{\infty} R^n \{u[t-(n+1)\tau] - u(t-n\tau)\}. \tag{6}$$

The first equation (1) is the local balance equation of the charge in the quantum well, and the second equation represents Kirchhoff's law of the circuit in which the device is operated. The control parameters are the external bias voltage U_0, the dimensionless load resistance r, and the timescale ratio $\varepsilon=RC/\tau_a$, which is related to the load resistance R, and the parallel capacitance C of the attached circuit, normalized by the tunneling time τ_a. A discussion of the various deterministic bifurcation scenarios can be found in [25,29,32].

We fix $\varepsilon=6.2$ slightly below the Hopf bifurcation, which occurs at $\varepsilon_{\mathrm{Hopf}} \approx 6.469$. In this regime we have two fixed points: (i) a stable, spatially inhomogeneous fixed point and (ii) a spatially homogeneous fixed point, which is stable with respect to completely homogeneous perturbations but generally unstable against spatially inhomogeneous fluctuations (saddle point). Although the deterministic system rests in the inhomogeneous steady state, noise can induce irregular spatiotemporal oscillations of the current density [8]. In the following we shall study how these noise-induced oscillations are influenced by the control force.

III. MULTIPLE TIME-DELAYED FEEDBACK CONTROL

Figure 1 shows simulations of the spatiotemporal dynamics under the influence of noise and delayed feedback. The voltage time series (a), the spatiotemporal charge density patterns (b), and the current-voltage projection of the

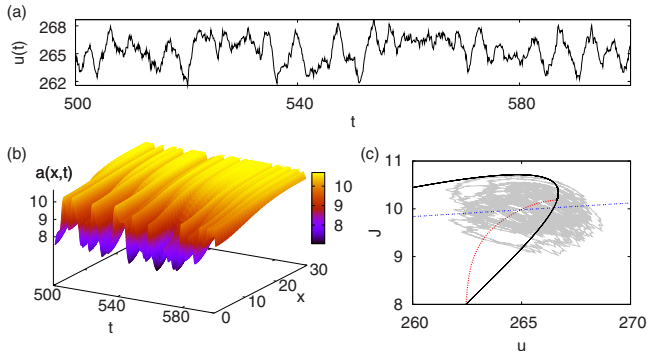

FIG. 2. (Color online) Same as Fig. 1 for $D_u=1.0$.

infinite-dimensional phase space (c) are depicted. Noise induces small *spatially inhomogeneous* oscillations around the inhomogeneous steady state (*breathing current filaments*). In the J-u phase portrait (c), the spatially inhomogeneous steady state (fixed point) is determined by the intersection of the load line (null isocline $\dot{u}=0$, blue dashed-dotted) with the nullcline $\dot{a}=0$ for inhomogeneous $a(x,t)$ (red dotted). The neighboring intersection of the load line with the nullcline $\dot{a}=0$ for homogeneous a (black solid curve) defines the second, spatially homogeneous fixed point, which is a saddle. With increasing noise intensity (Fig. 2) the oscillation amplitude becomes larger, the oscillations become more irregular, and finally, at even larger noise, the oscillations are more spatially homogeneous, i.e., in the phase space they are more centered around the homogeneous fixed point (Fig. 3).

We shall now investigate how the regularity and the time scales of these noise-induced oscillations depend upon the feedback parameters K, R, τ.

A. Linear stability analysis

To this purpose we first examine the stability properties of the inhomogeneous fixed point $(a_0(x),u_0)$ under the influence of the control force. We perform a linearization of the original continuous system (1) (with $D_u=D_a=0$) around the inhomogeneous fixed point along the same lines as in [22,33]. We use an exponential ansatz for the deviations from the fixed point $\delta a(x,t)\equiv a(x,t)-a_0(x)=e^{\Lambda t}\tilde{a}(x)$ and $\delta u(t)\equiv u(t)-u_0=e^{\Lambda t}\tilde{u}$. The resulting coupled eigenvalue problem reads

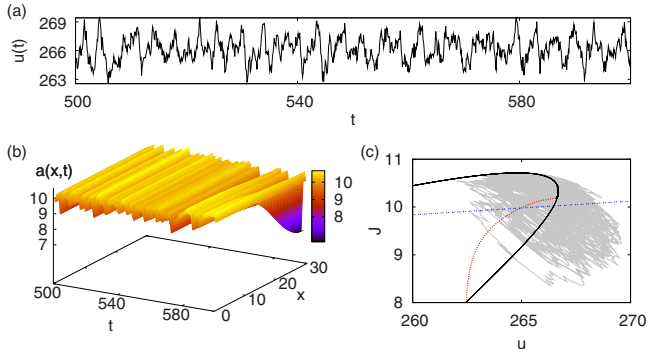

FIG. 3. (Color online) Same as Fig. 1 for $D_u=2.0$.

$$\Lambda\tilde{a}(x)=\hat{H}\tilde{a}(x)+f_u(x)\tilde{u}, \tag{7}$$

$$\Lambda\tilde{u}=-\frac{r}{\varepsilon L}\int_0^L j_a(x)\tilde{a}(x)dx-\frac{1+rJ_u}{\varepsilon}\tilde{u}-K\frac{1-e^{-\Lambda\tau}}{1-Re^{-\Lambda\tau}}\tilde{u}, \tag{8}$$

where we have introduced a self-adjoint linear operator

$$\hat{H}\equiv\left.\frac{\partial f}{\partial a}\right|_{a_0,u_0}+\left.\frac{\partial b}{\partial a}\right|_{a_0}+\left.\frac{\partial b}{\partial a_x}\right|_{a_0}\frac{\partial}{\partial x}+\left.\frac{\partial b}{\partial a_{xx}}\right|_{a_0}\frac{\partial^2}{\partial x^2}. \tag{9}$$

The index x denotes the partial derivative with respect to the spatial variable, and $b(a,a_x,a_{xx})=\frac{\partial}{\partial x}[D(a)a_x]$ is an abbreviation for the diffusion term in the first equation of the model system (1).

The eigenfunctions Ψ_i and eigenvalues λ_i of $\hat{H}$ correspond to the voltage-clamped system, $\delta u=0$. Furthermore,

$$f_u\equiv\left.\frac{\partial f}{\partial u}\right|_{a_0,u_0},\quad j_a\equiv\left.\frac{\partial j}{\partial a}\right|_{a_0,u_0},$$

$$J_u=\frac{1}{L}\int_0^L\left.\frac{\partial j}{\partial u}\right|_{a_0,u_0}dx. \tag{10}$$

Due to the global constraint, Eq. (8) mixes the eigenmodes Ψ_i and both equations have to be solved simultaneously. An expansion of the eigenmodes $\tilde{a}$ of the full system in terms of the eigenmodes Ψ_i of the voltage-clamped system, keeping only the dominant eigenmode Ψ_0 with eigenvalue $\lambda_0>0$, leads to a characteristic equation for the eigenvalues Λ,

$$\Lambda^2+\left(\frac{1+rJ_u}{\varepsilon}-\lambda_0\right)\Lambda+(\Lambda-\lambda_0)K\frac{1-e^{-\Lambda\tau}}{1-Re^{-\Lambda\tau}}-\frac{\lambda_0}{\varepsilon}(1+r\sigma_d)=0, \tag{11}$$

where the static differential conductance at the inhomogeneous fixed point $\sigma_d\equiv\left.\frac{dJ}{du}\right|_{a_0,u_0}$ has been introduced. In [22] a more detailed derivation of the characteristic equation is given for the special case $R=0$. The extension to the case $R\neq 0$ is straightforward.

Without control, $K=0$, Eq. (11) reduces to a characteristic polynomial of second order, which gives the well-known conditions for stability of a filament [33]

$$A\equiv\frac{1+rJ_u}{\varepsilon}-\lambda_0>0,$$

$$C\equiv-\frac{\lambda_0}{\varepsilon}(1+r\sigma_d)>0, \tag{12}$$

and a Hopf bifurcation occurs on the two-dimensional center manifold if $A=0$.

With control, Eq. (11) can be expressed as

$$\Lambda^2 + A\Lambda + (\Lambda - B)K\frac{1-e^{-\Lambda\tau}}{1-Re^{-\Lambda\tau}} + C = 0, \tag{13}$$

with $B \equiv \lambda_0 > 0$. The parameters A, B, C can be calculated directly from Eq. (12) [22], yielding $A=0.0447$, $B=1.0281$, and $C=1.1458$.

Using Eq. (13) we can calculate the domains of stability in the τ-K plane numerically for selected values of the memory parameter R. In order to find the curves containing the boundaries of stability of the inhomogeneous fixed point as a subset, we set $\Lambda=p+iq$ with $p=0$ and separate Eq. (13) into real and imaginary parts as follows:

$$[BK - R(C-q^2)]\cos(q\tau) - q(AR+K)\sin(q\tau) = BK + (q^2 - C), \tag{14}$$

$$q(AR+K)\cos(q\tau) + [BK + R(q^2-C)]\sin(q\tau) = q(A+K). \tag{15}$$

Using Eqs. (14) and (15) the boundary of stability can be obtained from the set of parametric functions $K(q)$ and $\tau(q)$ using $q=\mathrm{Im}(\Lambda)$ as the curve parameter:

$$K(q) = \frac{[A^2q^2 + (C-q^2)^2](1+R)}{2BC - 2(A+B)q^2},$$

$$\tau(q) = \frac{1}{q}\left(\arcsin\left(\frac{q(AB + C - q^2)(1-R)K}{[A^2q^2 + (C-q^2)^2]R^2 + 2[-BC + (A+B)q^2]RK + (B^2+q^2)K^2}\right) + 2\pi N\right). \tag{16}$$

Figure 4 shows these curves, Eq. (16), as blue lines. The boundaries of stability, where a delay-induced Hopf bifurcation of deterministic breathing oscillations occurs, are a subset of these curves, because the fixed point may already be unstable when a complex eigenvalue crosses the imaginary axis, due to other unstable eigenvalue branches. The boundaries are in good agreement with the domain of stability obtained from dynamical simulations of the nonlinear system equations (1) ($D_u=D_a=0$), shown as orange (dark shaded) areas. The inset of panel (c) shows the delay-induced limit cycle in the J-u phase space for parameters outside the stability domain of the inhomogeneous fixed point. The stability domains increase significantly with increasing memory parameter R from (a) to (d). The modulation of their boundaries in dependence on τ results from the crossover of different eigenvalue branches, which is a typical feature of delay differential equations.

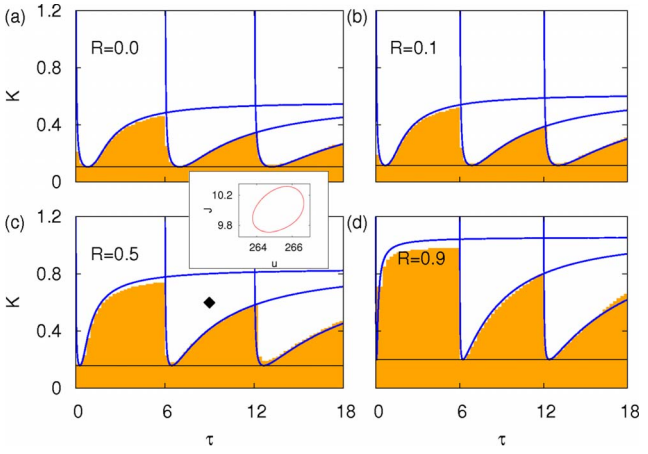

FIG. 4. (Color online) (a)–(d) Stability domains of the inhomogeneous fixed point in the τ-K plane of the deterministic system (1) ($D_u=D_a=0$), for selected values of the memory parameter R. Blue lines: Solutions of Eq. (13) with $\mathrm{Re}(\Lambda)=0$ calculcated from Eq. (16). Orange (shaded) region: Regime of stability of the fixed point obtained from the numerical solution of Eq. (1). Black horizontal line: Upper bound for K where the fixed point is stable for all values of τ, calculated from Eq. (17). The black diamond in panel (c) marks the parameter values for which a J-u phase portrait of the delay-induced limit cycle is shown in the inset.

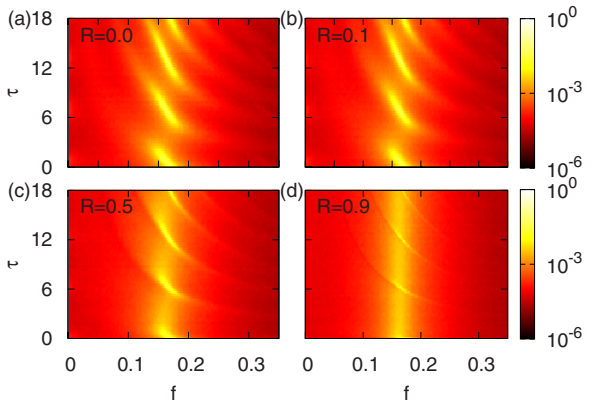

FIG. 5. (Color online) (a)–(d) Power spectral density $S_{uu}(f)$ of the dynamical variable u in dependence of the frequency f and the delay time τ for selected values of R ($K=0.1$, $\varepsilon=6.2$, $D_u=0.1$, $D_a=10^{-4}$).

From Eq. (16) it is possible to calculate an upper bound K_c of K for which the stability properties of the uncontrolled deterministic system remain unchanged over the whole τ interval, meaning that no delay-induced Hopf bifurcation occurs.

$$K_c = \frac{A^2(A+B)(BC-G)+(AC+G)^2}{2(A+B)^2G}(1+R)$$
$$\approx 0.1059(1+R),$$
$$G := \sqrt{A^2C[B(A+B)+C]}. \quad (17)$$

Figure 4 shows this upper bound plotted as a black horizontal line.

B. Correlation times

To quantify the temporal regularity of the noise-induced oscillations, we evaluate the correlation time [34] calculated from the voltage signal,

$$t_{\mathrm{cor}} \equiv \frac{1}{\sigma^2}\int_0^\infty |\Psi(s)|ds, \quad (18)$$

where $\Psi(s) \equiv \langle [u(t)-\langle u\rangle][u(t+s)-\langle u\rangle]\rangle_t$ is the autocorrelation function of the variable $u(t)$ and $\sigma^2=\Psi(0)$ its variance.

In order to investigate the influence of multiple time-delayed feedback control in the DBRT, we systematically study the dependence of the correlation time from Eq. (18) upon the control force parameters τ, K, and R.

In Fig. 5 the Fourier power spectral density S_{uu} obtained from the time series $u(t)$ is shown in dependence of the delay time τ for different values of the memory parameter R. The shape of the spectra $S_{uu}(2\pi f)$ alternates between broad and sharply peaked with varying τ. This shows up more clearly in the corresponding sections at fixed τ depicted in Fig. 6. A very good analytic approximation of the power spectral density can be obtained by a straightforward extension of the argument in [22] to multiple time-delayed feedback, with effective noise intensity $D' \ll 1$:

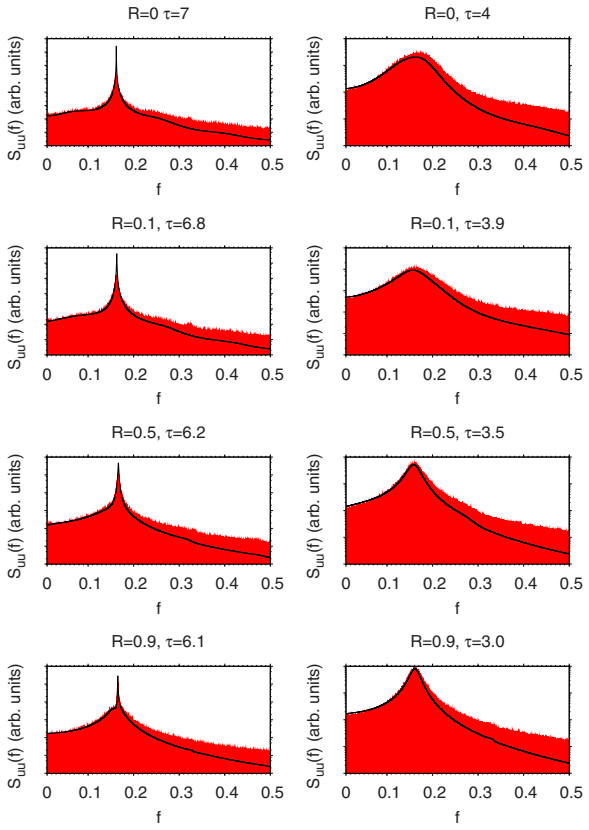

FIG. 6. (Color online) Power spectral density $S_{uu}(f)$ of the dynamical variable u in dependence of the frequency f for various delay times τ and memory parameters R (K=0.1, ε=6.2, D_u=0.1, $D_a=10^{-4}$).

$$S_{uu}(\omega) = \frac{D'^2}{2\pi}\left[\left(-\omega^2 + BK\frac{[\cos(\omega\tau)-1](R+1)}{1+R^2-2R\cos(\omega\tau)} - \frac{\omega K(1-R)\sin(\omega\tau)}{1+R^2-2R\cos(\omega\tau)} + C\right)^2 + \left(-A\omega + \omega K\frac{[\cos(\omega\tau)-1](R+1)}{1+R^2-2R\cos(\omega\tau)} + BK\frac{(1-R)\sin(\omega\tau)}{1+R^2-2R\cos(\omega\tau)}\right)^2\right]^{-1}, \quad (19)$$

which is shown as black curves in Fig. 6.

At certain resonant values of τ (left column) the spectral peaks become extremely sharp. With increasing memory parameter R the broad spectra prevail over larger intervals of τ, whereas the regime of sharply peaked spectra becomes smaller. Thus multiple time feedback control exhibits much more pronounced resonant features both in the frequency domain and in the delay time. Since a sharply peaked spectrum gives rise to long correlation times (which are, in the linear regime, proportional to the inverse spectral width) we expect the domains of strong correlation to shrink with increasing memory parameter and the domains of low correlation to increase. Extracting from the Fourier power spectral density the autocorrelation function $\Psi(s)=\int_{-\infty}^{\infty} S_{uu}(f)e^{2\pi i f s}df$ and using Eq. (18) we obtain the correlation time t_{cor} in dependence of τ. This is shown in Fig. 7 for different values of the memory parameter R. The feedback strength is kept at a constant value of K=0.1, where the system is below the Hopf bifurcation for all values of τ and R.

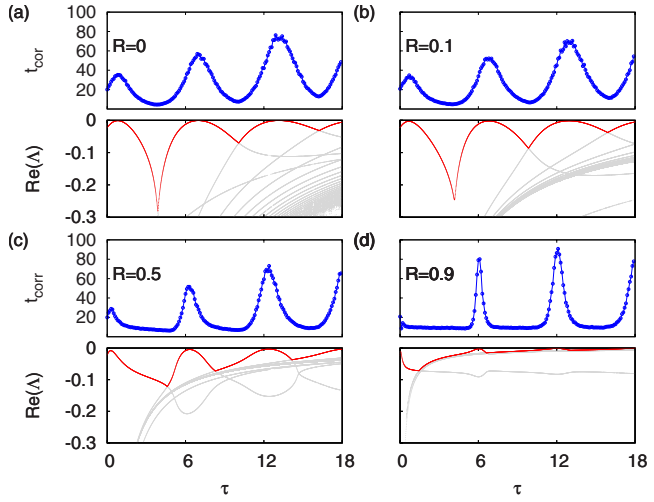

FIG. 7. (Color online) Correlation times t_{cor} (upper panels) and deterministic stability of the inhomogeneous fixed point, Re(Λ) (lower panels), in dependence of the delay time τ for different values of the memory parameter R [(a)–(d)] and fixed $K=0.1$. The red (dark) curves in the lower panels mark the leading eigenvalue, which governs the overall stability of the fixed point. Parameters: $\varepsilon=6.2$, $D_u=0.1$, and $D_a=10^{-4}$ (in the panels showing t_{cor}).

For small memory parameter R the correlation times alternate between high and low values with growing τ. For higher memory parameters R the peaks in correlation time indeed become narrower and sharpen up, and the domains of low correlation time increase. The stability of the inhomogeneous fixed point reveals a relation between properties of the controlled deterministic system and the noise-induced dynamics: maximum regularity of noise-induced oscillations is attained when the deterministic fixed point is least stable. This feature is maintained for all values of the memory parameter R. In the case of small R the crossover of the real part of eigenvalue branches also determines the location of the minima in correlation time. In that case two eigenmodes

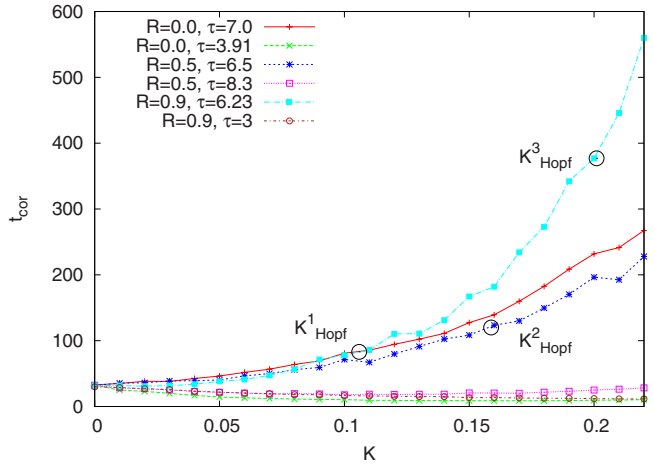

FIG. 8. (Color online) Correlation times t_{cor} in dependence of K for different values of the memory parameter R and optimal and nonoptimal τ ($\varepsilon=6.2$, $D_u=0.1$, $D_a=10^{-4}$). K^1_{Hopf}, K^2_{Hopf}, and K^3_{Hopf} mark the values of K at which the Hopf bifurcation occurs for $R=0$, $R=0.5$, and $R=0.9$, respectively ($\varepsilon=6.2$, $D_u=0.1$, $D_a=10^{-4}$).

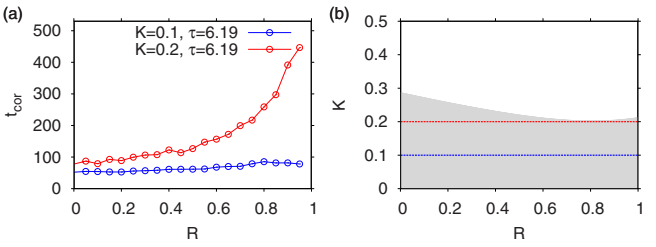

FIG. 9. (Color online) (a) Correlation times t_{cor} in dependence of the memory parameter R for different values of the coupling strength K and $\tau=6.19$. (b) Domain of stability of the inhomogeneous fixed point (green shaded) in the (K,R) plane for $\tau=6.19$. The horizontal lines mark the values of K chosen in (a) ($\varepsilon=6.2$, $D_u=0.1$, $D_a=10^{-4}$).

with the same stability (real part) but different frequencies are present in the system, resulting in rather irregular noise-induced dynamics. For large memory parameters the broad domains of low correlation display many eigenmodes that are not well separated (stability wise) causing irregular mixed dynamics.

The regularity of the noise-induced oscillations in dependence of the control force strength K is visualized in Fig. 8. The correlation time vs K is shown for different values of R and τ. Depending upon the chosen value of τ the correlation time increases or decreases with growing K. An optimal value of τ leads to more regular oscillations whereas a nonoptimal value of τ results in more irregular oscillations. In the case of an optimally chosen τ and a value of $K>0.1$ the curves split for larger K, and the one with largest R (blue full squares) attains the highest correlation times, clearly above the curves for $R=0$ (red plus) and $R=0.5$ (violet asterisks). Comparing the values of t_{cor} at the threshold of delay-induced Hopf bifurcation of the fixed point, marked by K^i_{Hopf}, the order of increasing correlation time is from small to large R.

The dependence of the correlation time on the memory parameter R is shown in Fig. 9(a) at a fixed value of τ

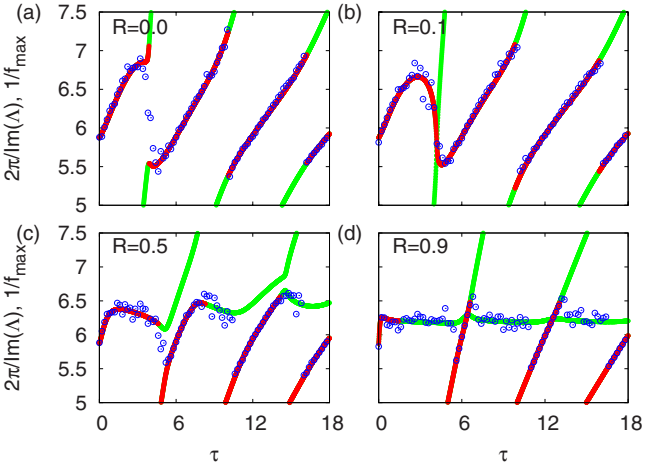

FIG. 10. (Color online) Main period $T_0=1/f_{max}$ of the noise-induced oscillations obtained from the main peak in the power spectral density (blue open circles). Red (solid) curve: Period $T=2\pi/\mathrm{Im}(\Lambda_0)$ of the leading eigenvalue. Green (gray) curves: Period $T=2\pi/\mathrm{Im}(\Lambda_i)$ ($K=0.1$, $\varepsilon=6.2$, $D_u=0.1$, $D_a=10^{-4}$).

=6.19 and values of $K=0.1$ and 0.2. Initially starting at a higher value of t_{cor} the correlation time increases more rapidly and reaches higher values in the case of larger K ($K=0.2$). Figure 9(b) shows the domain of stability in the K-R plane. The colored (dark) region is the domain where the inhomogeneous fixed point is stable under the influence of the feedback loop without noise. The two lines mark the chosen values of K used in Fig. 9(a). Again, the correlation time is maximum if the fixed point is closest to its boundary of stability.

C. Mean period

Here we will establish a relation between the linear modes of the inhomogeneous fixed point and the time scales of the noise-induced oscillations in its vicinity. The stability and angular frequency of the eigenmodes are given by the real and imaginary parts of the eigenvalues Λ_i of Eq. (13), $\mathrm{Re}(\Lambda_i)$ and $\mathrm{Im}(\Lambda_i)$, respectively. Figure 10 shows a plot of the main periods of the noise-induced oscillations obtained from the main peak in the Fourier power spectral density (blue open circles) compared to the periods calculated from the imaginary part $\mathrm{Im}(\Lambda_i)$ of the eigenvalues of the deterministic fixed point using Eq. (13). The red (solid) curve shows the periods $T_0=2\pi/\mathrm{Im}(\Lambda_0)$ of the leading eigenvalue. For small memory parameter R the period of the oscillations closely follows the eigenperiod corresponding to the leading eigenvalue over the whole τ interval, whereas for larger R this feature is only maintained in a narrow domain where the leading eigenvalue has a real part close to zero and is clearly separated from all other eigenmodes (compare Fig. 7).

IV. CONCLUSION

In conclusion, we have shown that multiple time-delayed feedback control leads to more pronounced resonant features of noise-induced spatiotemporal current oscillations in a semiconductor nanostructure compared to single time feedback. The regularity of noise-induced oscillations measured by the correlation time exhibits sharp resonances as a function of the delay time τ, and can be strongly increased by control with optimal choices of τ, whereas it decreases in a broad range of nonoptimal values of τ. Thus the system is more sensitive to variations in τ. Similarly, the peaks in the power spectral density are sharper and exhibit stronger resonances in dependence on τ for multiple time feedback, whereas their position, i.e., the main period of the oscillations, is less sensitive to variations in τ in wider intervals.

The regularity and time scales of noise-induced breathing oscillations are related to the stability properties of the deterministic stationary filamentary current pattern (fixed point) under the influence of the control loop. Maximum regularity is attained if the fixed point is least stable in the deterministic case. In the domains of high temporal correlation the period of the noise-induced oscillations corresponds to the eigenperiod of the leading eigenvalue in the deterministic system.

Furthermore, we have shown that using multiple time-delayed feedback control compared to single time-delayed feedback leads to larger regimes of stability of the stationary filamentary current pattern in the deterministic system, and delay-induced bifurcations occur only at larger values of the control amplitude K.

ACKNOWLEDGMENTS

This work was supported by DFG in the framework of Sfb 555. We are grateful to Grischa Stegemann for helpful discussions.

[1] Y. M. Blanter and M. Büttiker, Phys. Rep. **336**, 1 (2000).
[2] G. Giacomelli, M. Giudici, S. Balle, and J. R. Tredicce, Phys. Rev. Lett. **84**, 3298 (2000).
[3] V. V. Sherstnev, A. Krier, A. G. Balanov, N. B. Janson, A. N. Silchenko, and P. V. E. McClintock, Fluct. Noise Lett. **3**, L91 (2003).
[4] O. V. Ushakov, H. J. Wünsche, F. Henneberger, I. A. Khovanov, L. Schimansky-Geier, and M. A. Zaks, Phys. Rev. Lett. **95**, 123903 (2005).
[5] J. Hizanidis, A. G. Balanov, A. Amann, and E. Schöll, Phys. Rev. Lett. **96**, 244104 (2006).
[6] Hu Gang, T. Ditzinger, C. Z. Ning, and H. Haken, Phys. Rev. Lett. **71**, 807 (1993).
[7] A. S. Pikovsky and J. Kurths, Phys. Rev. Lett. **78**, 775 (1997).
[8] G. Stegemann, A. G. Balanov, and E. Schöll, Phys. Rev. E **71**, 016221 (2005).
[9] *Handbook of Chaos Control*, 2nd ed., edited by E. Schöll and H. G. Schuster (Wiley-VCH, Weinheim, 2008).
[10] N. B. Janson, A. G. Balanov, and E. Schöll, Phys. Rev. Lett. **93**, 010601 (2004).
[11] A. G. Balanov, N. B. Janson, and E. Schöll, Physica D **199**, 1 (2004).
[12] K. Pyragas, Phys. Lett. A **170**, 421 (1992).
[13] E. Schöll, A. G. Balanov, N. B. Janson, and A. Neiman, Stochastics Dyn. **5**, 281 (2005).
[14] J. Pomplun, A. Amann, and E. Schöll, Europhys. Lett. **71**, 366 (2005).
[15] B. Hauschildt, N. B. Janson, A. G. Balanov, and E. Schöll, Phys. Rev. E **74**, 051906 (2006).
[16] T. Prager, H. P. Lerch, L. Schimansky-Geier, and E. Schöll, J. Phys. A **40**, 11045 (2007).
[17] A. Pototsky and N. B. Janson, Phys. Rev. E **76**, 056208 (2007).
[18] A. Pototsky and N. B. Janson, Phys. Rev. E **77**, 031113 (2008).
[19] J. Hizanidis, A. G. Balanov, A. Amann, and E. Schöll, Int. J. Bifurcation Chaos Appl. Sci. Eng. **16**, 1701 (2006).
[20] A. G. Balanov, V. Beato, N. B. Janson, H. Engel, and E. Schöll, Phys. Rev. E **74**, 016214 (2006).
[21] M. Gassel, E. Glatt, and F. Kaiser, Phys. Rev. E **77**, 066220 (2008).
[22] G. Stegemann, A. G. Balanov, and E. Schöll, Phys. Rev. E **73**, 016203 (2006).
[23] J. E. S. Socolar, D. W. Sukow, and D. J. Gauthier, Phys. Rev.

E **50**, 3245 (1994).
[24] O. Beck, A. Amann, E. Schöll, J. E. S. Socolar, and W. Just, Phys. Rev. E **66**, 016213 (2002).
[25] J. Unkelbach, A. Amann, W. Just, and E. Schöll, Phys. Rev. E **68**, 026204 (2003).
[26] J. Schlesner, A. Amann, N. B. Janson, W. Just, and E. Schöll, Phys. Rev. E **68**, 066208 (2003).
[27] T. Dahms, P. Hövel, and E. Schöll, Phys. Rev. E **76**, 056201 (2007).
[28] J. Pomplun, A. G. Balanov, and E. Schöll, Phys. Rev. E **75**, 040101(R) (2007).
[29] E. Schöll, A. Amann, M. Rudolf, and J. Unkelbach, Physica B **314**, 113 (2002).
[30] E. Schöll, *Nonlinear Spatio-Temporal Dynamics and Chaos in Semiconductors* (Cambridge University Press, Cambridge, 2001).
[31] V. Cheianov, P. Rodin, and E. Schöll, Phys. Rev. B **62**, 9966 (2000).
[32] M. Meixner, P. Rodin, E. Schöll, and A. Wacker, Eur. Phys. J. B **13**, 157 (2000).
[33] A. Alekseev, S. Bose, P. Rodin, and E. Schöll, Phys. Rev. E **57**, 2640 (1998).
[34] R. L. Stratonovich, *Topics in the Theory of Random Noise* (Gordon and Breach, New York, 1963), Vol. 1.